INT. J. GEOGRAPHICAL INFORMATION SCIENCE, 1998, VOL. 12, NO. 8, 829–852

Research Article

Derivation of topographic variables from a digital elevation model given by a spheroidal trapezoidal grid

IGOR V. FLORINSKY
Institute of Mathematical Problems of Biology, Russian Academy of Sciences, Pushchino, Moscow Region, 142292, Russia
email: flor@impb.serpukhov.su

Abstract. Digital elevation models (DEMs) given by spheroidal trapezoidal grids are more appropriate for large regional, sub-continental, continental and global geological and soil studies than square-spaced DEMs. Here we develop a method for derivation of topographic variables, specifically horizontal (k_h) and vertical (k_v) landsurface curvatures, from spheroidal trapezoidal-spaced DEMs. First, we derive equations for calculation of partial derivatives of elevation with DEMs of this sort. Second, we produce formulae for estimation of the method accuracy in terms of root mean square errors of partial derivatives of elevation, as well as k_h and k_v (m_{kh} and m_{kv} respectively). We design the method for the case that the Earth's shape can be ignored, that is, for DEM grid sizes of no more than 225 km. We test the method by the example of fault recognition using a DEM of a part of Central Eurasia. A comparative analysis of test results and factual geological data demonstrates that the method actually works in regions marked by complicated topographic and tectonic conditions. Upon increasing DEM grid size, one can produce generalised maps of k_h and k_v. Spatial distributions of m_{kh} and m_{kv} depend directly on the distribution of elevation RMSE. Areas with high values of m_{kh} are marked by low values of m_{kv}, and vice versa, areas with high values of m_{kv} are marked by low values of m_{kh}. Data on m_{kh} and m_{kv} should be utilised to control and improve applications of k_h and k_v to geological studies. The method developed opens up new avenues for carrying out some 'conventional' raster operations directly on geographical co-ordinates.

1. Introduction

Topography influences migration and accumulation of substances moved by gravity along the landsurface and in the soil (Young 1972), microclimatic and meteorological characteristics (Geiger 1966), soil formation (Gerrard 1981), and vegetation cover properties (Yaroshenko 1961), and besides, relief is an indicator of geological structures, specifically faults (Ollier 1981). In this connection digital terrain models (DTMs) are used in soil, hydrological, plant, geomorphic and geological investigations (see detailed reviews by Moore *et al.* 1991, Shary *et al.* 1991, Florinsky 1998 b).

DTMs can be defined as digital representations of variables relating to a topographic surface, namely: digital elevation models (DEMs), digital models of gradient, aspect, horizontal (k_h) and vertical (k_v) landsurface curvatures, specific catchment area and other topographic attributes (Miller and Leflamme 1958, Burrough 1986, Felicisimo 1994, Shary 1995). Significant scientific and practical interest is being shown in data on k_h and k_v. k_v is the curvature of a normal section of the landsurface; this section includes a gravity acceleration vector at a given point on the landsurface.

1365-8816/98 $12.00

k_h is a curvature of a normal section of the landsurface; this section is orthogonal to the section with k_v (Sobolevsky 1932, Aandahl 1948, Evans 1972, Krcho 1973, Shary 1991).

k_h controls the range of convergence of overland and intrasoil flows: flows diverge when $k_h > 0$ while flows converge when $k_h < 0$ (Kirkby and Chorley 1967). k_v determines relative deceleration of overland and intrasoil flow movement: flows accelerate when $k_v > 0$ while flows decelerate when $k_v < 0$ (Speight 1974). Generally, mapping of k_h and k_v allows one to reveal ridge/valley spurs and terraces, respectively (Shary 1995). k_h and k_v utilisation and interpretation are possible over a wide range of scales. Data on k_h and k_v are used in detailed and large-scaled investigations and modelling of soil moisture (Troeh 1964, Kirkby and Chorley 1967, Burt and Butcher 1985, Feranec *et al.* 1991), thickness of soil horizons (Aandahl 1948, Pennock *et al.* 1987, Moore *et al.* 1993, Gessler *et al.* 1995), soil erosion (Martz and De Jong 1987), landslide distribution (Lanyon and Hall 1983), and plant cover (Florinsky and Kuryakova 1996). k_h and k_v models are applied to geomorphic studies in various scales (Kvietkauskas 1963–1964, Evans 1972, 1980, 1987, Franklin 1987, Dikau 1988, Guzzetti and Reichenbach 1994). Hand-derived k_h maps find use in middle- and small-scaled soil mapping (Anisimov *et al.* 1977, Stepanov 1979, 1989). Stepanov (1986) and Kuryakova and Florinsky (1991) utilised hand-derived k_h maps to investigate regularities of spatial interrelations between geological structures, landforms and soil cover in regional and sub-continental scales. Finally, k_h and k_v digital models can be used to reveal faults, geological lineaments and ring structures (Florinsky 1992), and to recognise fault morphology (Florinsky 1996) at different scales.

Once elevations are given by $z = f(x, y)$ where x and y are plane Cartesian co-ordinates, k_h and k_v are functions of the partial derivatives of z (Shary 1991):

$$k_h = -\frac{q^2 r - 2pqs + p^2 t}{(p^2 + q^2)\sqrt{1 + p^2 + q^2}} \tag{1}$$

$$k_v = -\frac{p^2 r + 2pqs + q^2 t}{(p^2 + q^2)\sqrt{(1 + p^2 + q^2)^3}} \tag{2}$$

where

$$r = \frac{\partial^2 z}{\partial x^2},\ t = \frac{\partial^2 z}{\partial y^2},\ s = \frac{\partial^2 z}{\partial x\, \partial y},\ p = \frac{\partial z}{\partial x},\ q = \frac{\partial z}{\partial y}. \tag{3}$$

One can calculate r, t, s, p and q with square-spaced DEMs by some methods (e.g. Evans 1979, Zevenbergen and Thorne 1987, Moore *et al.* 1993). The method of Evans (1979) has received wide acceptance owing to the ease and fast data processing, and high calculation accuracy (Florinsky 1998 a).

In the Evans method, the polynomial

$$z = \frac{rx^2}{2} + \frac{ty^2}{2} + sxy + px + qy + u \tag{4}$$

is approximated by the least squares method (§2) to the 3 by 3 square-spaced altitude submatrix with a grid size of w (figure 1 (*a*)). Points of the submatrix $(-w, w, z_1)$, $(0, w, z_2)$, (w, w, z_3), $(-w, 0, z_4)$, $(0, 0, z_5)$, $(w, 0, z_6)$, $(-w, w, z_7)$, $(0, -w, z_8)$ and $(w, -w, z_9)$ are measured plane Cartesian co-ordinates and elevations of the

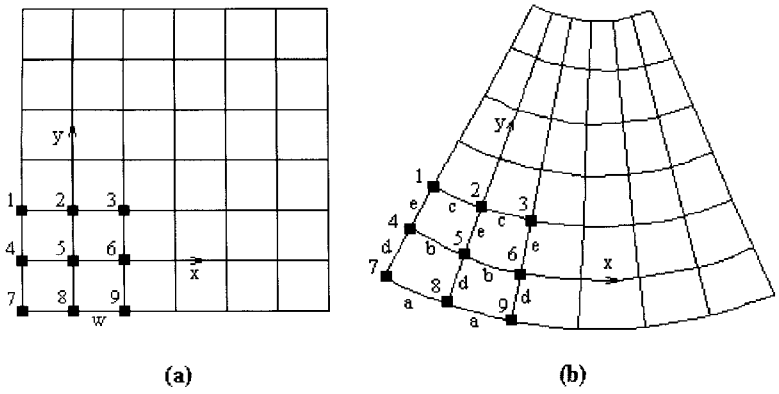

Figure 1. (*a*) submatrix for a square-spaced DEM: 1, ..., 9 are numbers of the submatrix nodes, w is a grid size in metres, (*b*) submatrix for a DEM given by a spheroidal trapezoidal grid: 1, ..., 9 are numbers of the submatrix nodes, a, b and c are lengths of parallel arcs in metres, d and e are lengths of meridian arcs in metres.

landsurface. As a result, we can estimate values of r, t, s, p and q at the point $(0, 0, z_5)$ by the following formulae:

$$r=\frac{z_1+z_3+z_4+z_6+z_7+z_9-2(z_2+z_5+z_8)}{3w^2}, \tag{5}$$

$$t=\frac{z_1+z_2+z_3+z_7+z_8+z_9-2(z_4+z_5+z_6)}{3w^2}, \tag{6}$$

$$s=\frac{z_3+z_7-z_1-z_9}{4w^2}, \tag{7}$$

$$p=\frac{z_3+z_6+z_9-z_1-z_4-z_7}{6w}, \tag{8}$$

$$q=\frac{z_1+z_2+z_3-z_7-z_8-z_9}{6w}. \tag{9}$$

Moving the 3 by 3 submatrix along a regular DEM, we can calculate values of r, t, s, p and q for all points of the DEM, excepting boundary points. We do not present a formula for the absolute term u in the polynomial (equation (4)), since u is not used in calculation of k_h and k_v. Notice that Sharpnack and Akin (1969) proposed expressions for p and q identical with equations (8 and 9). Equations (5–9) can be derived in the same fashion that we use in §2.

Equations (1–3) are true for landsurface areas when the Earth's sphericity can be ignored (Shary 1991). Therefore, digital models and maps of k_h and k_v described relatively local properties of the landsurface but do not consider the Earth's shape. We assume that this shape can be neglected if an area has a distance of no more than about $0.1R_E$ where R_E is the Earth's average radius, $R_E \approx 6378$ km (e.g. Bugaevsky and Vakhrameyeva 1992). This limitation pertains only to the submatrix size as one can use the principle of a moving submatrix to estimate k_h and k_v (see above). The submatrix size cannot be more than about 450 km by 450 km as a submatrix diagonal is no more than about 640 km. So, equations (1–3) can be used

if DEMs have grid sizes of no more than about 225 km. We should stress that the overall size of a territory under study can be as large as is wished.

However, the geometry of *square-spaced* grids of the 3 by 3 submatrix (figure 1 (*a*)) and DEMs suitable for the Evans method sets limits both on the overall size of a studied terrain and on the properties of topographic maps utilised for DEM compilation. Indeed, one can use the Evans method (equation (5–9)) if and only if the horizontal projection of a defined square-spaced altitude grid is also a square-spaced grid. This can be met for DEMs obtained by (*a*) conventional ground topographic surveys (Modrinsky 1972), (*b*) photogrammetric processing of two overlapping aerial orthoimages (Bobir *et al.* 1974), and (*c*) digitising contours of topographic maps (Kumler 1994) given in projections marked by minimum distortions in conformality and distance.

Two closely related conformal projections meet the latest condition, namely: the Gauss-Krüger and the Universal Transverse Mercator (UTM) projections (Bugaevsky and Vakhrameyeva 1992). The Gauss-Krüger projection is applied to compile topographic maps of 1:2000–1:500 000 scales in Russia while the UTM is commonly used for topographic mapping in other countries. With these projections, the spheroidal surface is divided into 6° zones by meridians. Each of these zones is mapped individually. Distance distortions increase away from the central meridian of a zone. For example, at 6° zone boundaries the Gauss-Krüger projection offers distance overestimation of 0.0009, 0.0006, 0.0004 and 0.0003 for parallels of 40°, 50°, 60° and 70°, respectively (Salishchev 1990). So, distance distortion can be ignored for each of 6° zones. Based on the feasible size of a territory lying within a 6° zone, one can apply its DTM to detailed and regional soil, hydrological, plant, geomorphic and geological investigations.

The Evans method is not appropriate for use in at least two cases:

1. If one carries out geological or soil study of a sizeable area located within two or more 6° zones. Although a DEM may be compiled by portions related to 6° zones, difficulties ensue with accurate jointing of adjacent sub-DEMs. Also, although the Evans method may be applied to derive k_h and k_v models from sub-DEMs, there is a problem of linking of k_h and k_v sub-models. This is because r, t, s, p and q are not calculated for DEM boundary points (see above). This causes 'blank strips' between adjacent sub-DTMs. Besides, a sub-DTM can be too small. For example, near the equator a sub-DEM and a k_h sub-model can include about 100 and 64 points, correspondingly, for an area measuring 6° by 4° and $w=55$ km.

2. If to compile a DEM for a small-scaled geological or soil study one uses maps with significant distortions in conformality and distance, such as 1:1 000 000 topographic maps given in the modified polyconic projection (Bugaevsky and Vakhrameyeva 1992). In this case, the horizontal projection of a defined square-spaced altitude grid is not a square-spaced grid. Besides, projection distortions can lead to artefacts in geological studies (Carey 1988), for example, through rectilinear lineaments, faults and other geological patterns can be mapped as curvilinear ones (Ollier 1981). Although one may resolve these difficulties by relevant transformations of a DEM projection, errors can arise in the transformed DEM due to elevation interpolation (Schut 1976).

In our opinion, the best solution of the problems discussed is to process immediately *spheroidal trapezoidal-spaced* DEMs rather than *square-spaced* ones for k_h and k_v derivation in large regional, sub-continental, continental and global geological and soil studies. This is because DEMs given by spheroidal trapezoidal grids (*a*) are

free of projection distortions, (*b*) can be compiled for sizeable areas without radical difficulties, and (*c*) may ideally be free of interpolation errors. Nodes of these DEMs relate to parallel and meridian intersections (figure 1 (*b*)). One can readily estimate the spatially varying DEM grid size (lengths of trapezoidal bases and legs), since parallel and meridian arc lengths are known (e.g. Bugaevsky and Vakhrameyeva 1992). Generally, spheroidal trapezoidal-spaced DEMs are described in the spherical (geographical) co-ordinate system. Obviously, one can describe square-spaced DEMs in the geographical co-ordinates too, but a spheroidal trapezoidal-spaced grid and a square-spaced one are marked by radically different geometry (figure 1).

The objective of this study is to develop a method for derivation of topographic variables, specifically k_h and k_v, from DEMs given by spheroidal trapezoidal grids. We cover the case that the Earth's shape is ignored, that is, DEM grid sizes of no more than 225 km. First, we derive equations for calculation of r, t, s, p and q with spheroidal trapezoidal-spaced DEMs. Second, we produce formulae for estimating accuracy in terms of root mean square errors (RMSE) of r, t, s, p and q, as well as k_h and k_v. Third, we test the method by the example of fault recognition using a DEM of a part of Central Eurasia.

2. Calculation of *r*, *t*, *s*, *p* and *q* with DEMs given by a spheroidal trapezoidal grid

Assume that elevations are given by $z=f(x, y)$ where x and y are spherical orthogonal co-ordinates. Let there be a 3 by 3 submatrix with nodes relating to apices of four adjacent spheroidal trapeziums that lie in the Earth's spheroid or ellipsoid surface. Two trapeziums have bases of a and b and legs of d, while two other trapeziums have bases of b and c and legs of e. a, b and c are lengths of parallel arcs in metres, while d and e are lengths of meridian arcs in metres (figure 1 (*b*)). Points of the submatrix $(-c, e, z_1)$, $(0, e, z_2)$, (c, e, z_3), $(-b, 0, z_4)$, $(0, 0, z_5)$, $(b, 0, z_6)$, $(-a, -d, z_7)$, $(0, -d, z_8)$ and $(a, -d, z_9)$ are measured spherical orthogonal co-ordinates and elevations of the landsurface. We ignore the Earth's shape within the submatrix, that is a, b, c, d and e are no more than 225 km (§1).

To develop formulae for derivation of r, t, s, p and q from a DEM given by a spheroidal trapezoidal grid let us approximate the polynomial (equation (4)) to the submatrix (figure 1 (*b*)) by the least squares method (Bronstein and Semendyaev 1956, Bjerhammar 1973). With this method, if we can estimate values of f_i of some functions $\varphi_i(x_1, x_2, ..., x_n)$, $i=1, 2, ..., m$, of unknowns $x_1, x_2, ..., x_n$, so to determine unknowns we should solve a system of so-called conditional equations $\varphi_i(x_1, x_2, ..., x_n)-f_i=0$. This is the incompatible equation system for $m>n$. Therefore, we can estimate only the most probable values of unknowns. A sum of deviation squared $\varepsilon_i=\varphi_i-f_i$ is the least for this case. If the conditional equations are linear ones:

$$\begin{cases} a_1x_1+b_1x_2+\cdots+l_1x_n=f_1 \\ a_2x_1+b_2x_2+\cdots+l_2x_n=f_2 \\ \cdots\cdots\cdots\cdots\cdots\cdots\cdots\cdots\cdots \\ a_mx_1+b_mx_2+\cdots+l_mx_n=f_m \end{cases}, \tag{10}$$

so to accomplish a minimum for the sum of deviations squared we should solve a

system of so-called normal linear equations:

$$\begin{cases} x_1 \sum_{i=1}^{m} a_i a_i + x_2 \sum_{i=1}^{m} a_i b_i + \cdots + x_n \sum_{i=1}^{m} a_i l_i = \sum_{i=1}^{m} a_i f_i \\ x_1 \sum_{i=1}^{m} b_i a_i + x_2 \sum_{i=1}^{m} b_i b_i + \cdots + x_n \sum_{i=1}^{m} b_i l_i = \sum_{i=1}^{m} b_i f_i \\ \cdots\cdots\cdots\cdots\cdots\cdots\cdots\cdots\cdots\cdots\cdots\cdots\cdots\cdots\cdots\cdots\cdots\cdots \\ x_1 \sum_{i=1}^{m} l_i a_i + x_2 \sum_{i=1}^{m} l_i b_i + \cdots + x_n \sum_{i=1}^{m} l_i l_i = \sum_{i=1}^{m} l_i f_i \end{cases}. \tag{11}$$

The convenient way to do this is through approaches of matrix algebra (Bjerhammar 1973). The equation system (10) can be transcribed using matrix symbols as

$$F\beta = \alpha \tag{12}$$

where β is a $n \times 1$ matrix of unknowns:

$$\beta = \begin{Vmatrix} x_1 \\ x_2 \\ \cdots \\ x_n \end{Vmatrix}, \tag{13}$$

α is a $m \times 1$ matrix of estimated values of f_i:

$$\alpha = \begin{Vmatrix} f_1 \\ f_2 \\ \cdots \\ f_m \end{Vmatrix}, \tag{14}$$

and F is a $m \times n$ matrix of known coefficients:

$$F = \begin{Vmatrix} a_1 & b_1 & \cdots & l_1 \\ a_2 & b_2 & \cdots & l_2 \\ \cdots & \cdots & \cdots & \cdots \\ a_m & b_m & \cdots & l_m \end{Vmatrix}. \tag{15}$$

The equation system (11) can be written as

$$F'F\beta = F'\alpha \tag{16}$$

where F' is a transposed matrix of the matrix F. Solving the equation (16) for β gives:

$$\beta=(F'F)^{-1}F'\alpha \tag{17}$$

where $(F'F)^{-1}$ is an inverse matrix of the matrix $F'F$.

To determine unknowns r, t, s, p and q let us write the polynomial (equation (4)) for the nine points of the 3 by 3 submatrix. As a result, we can derive nine conditional equations of the form:

$$z_i=\frac{rx_i^2}{2}+\frac{ty_i^2}{2}+sx_iy_i+px_i+qy_i+u \tag{18}$$

where x_i, y_i and z_i are measured spherical orthogonal co-ordinates and elevations of the submatrix points, $i=1, ..., 9$. Therefore, we obtain the following system of nine conditional linear equations:

$$\begin{cases} z_1=\frac{c^2}{2}r+\frac{e^2}{2}t-ces-cp+eq+u \\ z_2=\frac{e^2}{2}t+eq+u \\ z_3=\frac{c^2}{2}r+\frac{e^2}{2}t+ces+cp+eq+u \\ z_4=\frac{b^2}{2}r-bp+u \\ z_5=u \\ z_6=\frac{b^2}{2}r+bp+u \\ z_7=\frac{a^2}{2}r+\frac{d^2}{2}t+ads-ap-dq+u \\ z_8=\frac{d^2}{2}t-dq+u \\ z_9=\frac{a^2}{2}r+\frac{d^2}{2}t-ads+ap-dq+u. \end{cases} \tag{19}$$

In this case, β is a 6×1 matrix of six unknown coefficients of the polynomial (equation (4)):

$$\beta=\begin{Vmatrix} r \\ t \\ s \\ p \\ q \\ u \end{Vmatrix}, \tag{20}$$

α is a 9×1 matrix of nine measured elevations of the submatrix points:

$$\alpha = \begin{Vmatrix} z_1 \\ z_2 \\ z_3 \\ z_4 \\ z_5 \\ z_6 \\ z_7 \\ z_8 \\ z_9 \end{Vmatrix}, \tag{21}$$

and F is a 9×6 matrix of known coefficients of the equation system (19):

$$F = \begin{Vmatrix} \frac{c^2}{2} & \frac{e^2}{2} & -ce & -c & e & 1 \\ 0 & \frac{e^2}{2} & 0 & 0 & e & 1 \\ \frac{c^2}{2} & \frac{e^2}{2} & ce & c & e & 1 \\ \frac{b^2}{2} & 0 & 0 & -b & 0 & 1 \\ 0 & 0 & 0 & 0 & 0 & 1 \\ \frac{b^2}{2} & 0 & 0 & b & 0 & 1 \\ \frac{a^2}{2} & \frac{d^2}{2} & ad & -a & -d & 1 \\ 0 & \frac{d^2}{2} & 0 & 0 & -d & 1 \\ \frac{a^2}{2} & \frac{d^2}{2} & -ad & a & -d & 1 \end{Vmatrix}. \tag{22}$$

Through matrix and simple algebraic operations we can obtain the following 6×9 matrix $(F'F)^{-1}F'$:

$$(F'F)^{-1}F'=\left\|\begin{array}{ccc}
\dfrac{c^2}{a^4+b^4+c^4} & -\dfrac{2c^2}{a^4+b^4+c^4} & \dfrac{c^2}{a^4+b^4+c^4} \\
\dfrac{2[d(a^4+b^4+b^2c^2)-c^2e(a^2-b^2)]}{3de(d+e)(a^4+b^4+c^4)} & \dfrac{2[d(a^4+b^4+3c^4-2b^2c^2)+2c^2e(a^2-b^2)]}{3de(d+e)(a^4+b^4+c^4)} & \dfrac{2[d(a^4+b^4+b^2c^2)-c^2e(a^2-b^2)]}{3de(d+e)(a^4+b^4+c^4)} \\
-\dfrac{c[a^2(d+e)+b^2e]}{2[a^2c^2(d+e)^2+b^2(a^2d^2+c^2e^2)]} & 0 & \dfrac{c[a^2(d+e)+b^2e]}{2[a^2c^2(d+e)^2+b^2(a^2d^2+c^2e^2)]} \\
-\dfrac{a^2cd(d+e)}{2[a^2c^2(d+e)^2+b^2(a^2d^2+c^2e^2)]} & 0 & \dfrac{a^2cd(d+e)}{2[a^2c^2(d+e)^2+b^2(a^2d^2+c^2e^2)]} \\
\dfrac{d^2(a^4+b^4+b^2c^2)+c^2e^2(a^2-b^2)}{3de(d+e)(a^4+b^4+c^4)} & \dfrac{d^2(a^4+b^4+3c^4-2b^2c^2)-2c^2e^2(a^2-b^2)}{3de(d+e)(a^4+b^4+c^4)} & \dfrac{d^2(a^4+b^4+b^2c^2)+c^2e^2(a^2-b^2)}{3de(d+e)(a^4+b^4+c^4)} \\
-\dfrac{b^2c^2}{3(a^4+b^4+c^4)} & \dfrac{2b^2c^2}{3(a^4+b^4+c^4)} & -\dfrac{b^2c^2}{3(a^4+b^4+c^4)}
\end{array}\right.$$

$$\left.\begin{array}{ccc}
\dfrac{b^2}{a^4+b^4+c^4} & -\dfrac{2b^2}{a^4+b^4+c^4} & \dfrac{b^2}{a^4+b^4+c^4} \\
-\dfrac{2[d(a^4+c^4+b^2c^2)+e(a^4+c^4+a^2b^2)]}{3de(d+e)(a^4+b^4+c^4)} & -\dfrac{2[(a^4+3b^4+c^4)(d+e)-2b^2(a^2e+c^2d)]}{3de(d+e)(a^4+b^4+c^4)} & -\dfrac{2[d(a^4+c^4+b^2c^2)+e(a^4+c^4+a^2b^2)]}{3de(d+e)(a^4+b^4+c^4)} \\
-\dfrac{b(a^2d-c^2e)}{2[a^2c^2(d+e)^2+b^2(a^2d^2+c^2e^2)]} & 0 & \dfrac{b(a^2d-c^2e)}{2[a^2c^2(d+e)^2+b^2(a^2d^2+c^2e^2)]} \\
-\dfrac{b(a^2d^2+c^2e^2)}{2[a^2c^2(d+e)^2+b^2(a^2d^2+c^2e^2)]} & 0 & \dfrac{b(a^2d^2+c^2e^2)}{2[a^2c^2(d+e)^2+b^2(a^2d^2+c^2e^2)]} \\
-\dfrac{d^2(a^4+c^4+b^2c^2)-e^2(a^4+c^4+a^2b^2)}{3de(d+e)(a^4+b^4+c^4)} & -\dfrac{(a^4+3b^4+c^4)(d^2-e^2)+2b^2(a^2e^2-c^2d^2)}{3de(d+e)(a^4+b^4+c^4)} & -\dfrac{d^2(a^4+c^4+b^2c^2)-e^2(a^4+c^4+a^2b^2)}{3de(d+e)(a^4+b^4+c^4)} \\
\dfrac{a^4+c^4}{3(a^4+b^4+c^4)} & \dfrac{a^4+3b^4+c^4}{3(a^4+b^4+c^4)} & \dfrac{a^4+c^4}{3(a^4+b^4+c^4)}
\end{array}\right.$$

$$\left\|\begin{array}{ccc}
\dfrac{a^2}{a^4+b^4+c^4} & -\dfrac{2a^2}{a^4+b^4+c^4} & \dfrac{a^2}{a^4+b^4+c^4} \\
\dfrac{2[e(b^4+c^4+a^2b^2)+a^2d(b^2-c^2)]}{3de(d+e)(a^4+b^4+c^4)} & \dfrac{2[e(3a^4+b^4+c^4-2a^2b^2)-2a^2d(b^2-c^2)]}{3de(d+e)(a^4+b^4+c^4)} & \dfrac{2[e(b^4+c^4+a^2b^2)+a^2d(b^2-c^2)]}{3de(d+e)(a^4+b^4+c^4)} \\
\dfrac{a[c^2(d+e)+b^2d]}{2[a^2c^2(d+e)^2+b^2(a^2d^2+c^2e^2)]} & 0 & -\dfrac{a[c^2(d+e)+b^2d]}{2[a^2c^2(d+e)^2+b^2(a^2d^2+c^2e^2)]} \\
-\dfrac{ac^2e(d+e)}{2[a^2c^2(d+e)^2+b^2(a^2d^2+c^2e^2)]} & 0 & \dfrac{ac^2e(d+e)}{2[a^2c^2(d+e)^2+b^2(a^2d^2+c^2e^2)]} \\
-\dfrac{e^2(b^4+c^4+a^2b^2)-a^2d^2(b^2-c^2)}{3de(d+e)(a^4+b^4+c^4)} & -\dfrac{e^2(3a^4+b^4+c^4-2a^2b^2)+2a^2d^2(b^2-c^2)}{3de(d+e)(a^4+b^4+c^4)} & -\dfrac{e^2(b^4+c^4+a^2b^2)-a^2d^2(b^2-c^2)}{3de(d+e)(a^4+b^4+c^4)} \\
-\dfrac{a^2b^2}{3(a^4+b^4+c^4)} & \dfrac{2a^2b^2}{3(a^4+b^4+c^4)} & -\dfrac{a^2b^2}{3(a^4+b^4+c^4)}
\end{array}\right\| \tag{23}$$

Then, through simple algebraic operations we can solve the equation (17) and obtain the following formulae for calculation of r, t, s, p and q with spheroidal trapezoidal-spaced DEMs:

$$r=\frac{c^2(z_1+z_3-2z_2)+b^2(z_4+z_6-2z_5)+a^2(z_7+z_9-2z_8)}{a^4+b^4+c^4} \tag{24}$$

$$t=\frac{\begin{array}{l}2\{[d(a^4+b^4+b^2c^2)-c^2e(a^2-b^2)](z_1+z_3)-[d(a^4+c^4+b^2c^2)+e(a^4+c^4+a^2b^2)](z_4+z_6)+\\ +[e(b^4+c^4+a^2b^2)+a^2d(b^2-c^2)](z_7+z_9)+d[b^4(z_2-3z_5)+c^4(3z_2-z_5)+(a^4-2b^2c^2)(z_2-z_5)]+\\ +e[a^4(3z_8-z_5)+b^4(z_8-3z_5)+(c^4-2a^2b^2)(z_8-z_5)]-2[a^2d(b^2-c^2)z_8-c^2e(a^2-b^2)z_2]\}\end{array}}{3de(d+e)(a^4+b^4+c^4)} \tag{25}$$

$$s=\frac{c[a^2(d+e)+b^2e](z_3-z_1)-b(a^2d-c^2e)(z_4-z_6)+a[c^2(d+e)+b^2d](z_7-z_9)}{2[a^2c^2(d+e)^2+b^2(a^2d^2+c^2e^2)]} \quad (26)$$

$$p=\frac{a^2cd(d+e)(z_3-z_1)+b(a^2d^2+c^2e^2)(z_6-z_4)+ac^2e(d+e)(z_9-z_7)}{2[a^2c^2(d+e)^2+b^2(a^2d^2+c^2e^2)]} \quad (27)$$

$$q=\frac{[d^2(a^4+b^4+b^2c^2)+c^2e^2(a^2-b^2)](z_1+z_3)-[d^2(a^4+c^4+b^2c^2)-e^2(a^4+c^4+a^2b^2)](z_4+z_6)-}{-[e^2(b^4+c^4+a^2b^2)-a^2d^2(b^2-c^2)](z_7+z_9)+d^2[b^4(z_2-3z_5)+c^4(3z_2-z_5)+(a^4-2b^2c^2)(z_2-z_5)]+}{+e^2[a^4(z_5-3z_8)+b^4(3z_5-z_8)+(c^4-2a^2b^2)(z_5-z_8)]-2[a^2d^2(b^2-c^2)z_8+c^2e^2(a^2-b^2)z_2]} \quad (28)$$

$$3de(d+e)(a^4+b^4+c^4)$$

We do not present a formula for the absolute term u in the polynomial (equation (4)), since u is not used in calculation of k_h and k_v. We produced the equation (23) with the software Maple V 3.0 for Microsoft Windows.

As in the Evans method, the polynomial (equation (4)) is *approximated* to elevation values of the 3 by 3 submatrix (figure 1 (*b*)) rather than *passes exactly* through these values. This leads to some local filtering of high-frequency noise resulting from small random errors in DEM compilation (Shary 1995). This can correct calculation of derivatives because they are very responsive to high-frequency component of a signal (e.g. Pratt 1978). Surplus data are a further merit of the method developed: nine elevation values are used to estimate six coefficients of the polynomial (equation (4)). This improves the accuracy and tolerance of computations (Bugaevsky, personal communication 1993).

3. Accuracy of r, t, s, p, q, k_h and k_v calculated by the method developed

Let us estimate the precision of the method developed. r, t, s, p and q (equations (24–28)) are functions F of measured variables $F=\varphi(x, y, ..., u)$ where $x, y, ..., u$ are measured arguments, that is, z_i, $i=1, ..., 9$. The RMSE of $F(m_F)$ would be appropriate to evaluate the calculation accuracy of r, t, s, p and q (Kuryakova 1996, Florinsky 1998a). To estimate m_F the following formula can be applied (Gaidaev and Bolshakov 1969, p. 129):

$$m_F=\sqrt{\left(\frac{\partial F}{\partial x}\right)_0^2 m_x^2+\left(\frac{\partial F}{\partial y}\right)_0^2 m_y^2+\cdots+\left(\frac{\partial F}{\partial u}\right)_0^2 m_u^2} \quad (29)$$

where $m_x, m_y, ..., m_u$ are RMSE of $x, y, ..., u$, respectively.

Let us produce formulae of RMSE for r, t, s, p and q (m_r, m_t, m_s, m_p and m_q, respectively) with the equation (29). In particular,

$$m_r=\sqrt{\left(\frac{\partial r}{\partial z_1}\right)_0^2 m_{z_1}^2+\left(\frac{\partial r}{\partial z_2}\right)_0^2 m_{z_2}^2+\left(\frac{\partial r}{\partial z_3}\right)_0^2 m_{z_3}^2+\cdots+\left(\frac{\partial r}{\partial z_9}\right)_0^2 m_{z_9}^2} \quad (30)$$

where $m_{z_1}, m_{z_2}, m_{z_3}, ..., m_{z_9}$ are RMSE of $z_1, z_2, z_3, ..., z_9$, correspondingly. In the strict sense, $m_{z_i}=\psi(x, y)$ where x and y are spherical orthogonal co-ordinates. m_{z_i} depends on geomorphic conditions and a method of DEM compilation (Hunter and

Goodchild 1995). However, for a DEM produced by interpolation of digitised contours

$$m_{z_i} = const = B\Delta z \tag{31}$$

where $B = 0.16$–0.33, Δz is a contour interval (Li 1994). The factor B depends on geomorphic conditions, and the extent to which additional data on specific features (i.e. peaks and thalvegs) are taking into consideration in the DEM compilation. So, let us consider $m_{z_1} = m_{z_2} = \cdots = m_{z_9} = m_z$. Substituting m_z into the equation (30) gives:

$$m_r = m_z \sqrt{\left(\frac{\partial r}{\partial z_1}\right)_0^2 + \left(\frac{\partial r}{\partial z_2}\right)_0^2 + \left(\frac{\partial r}{\partial z_3}\right)_0^2 + \cdots + \left(\frac{\partial r}{\partial z_9}\right)_0^2} \tag{32}$$

Through differentiation and simple algebraic operations, we obtain the following expression of m_r:

$$m_r = m_z \sqrt{\frac{6}{a^4 + b^4 + c^4}} \tag{33}$$

In a similar manner, we derive the required expressions of m_t, m_s, m_p and m_q:

$$m_t = 2m_z \frac{\sqrt{2\{[d(a^4+b^4+b^2c^2) - c^2e(a^2-b^2)]^2 + [d(a^4+c^4+b^2c^2) + e(a^4+c^4+a^2b^2)]^2 + [e(b^4+c^4+a^2b^2) + a^2d(b^2-c^2)]^2\} + [d(a^4+b^4+3c^4-2b^2c^2) + 2c^2e(a^2-b^2)]^2 + [2b^2(a^2e+c^2d) - (a^4+3b^4+c^4)(d+e)]^2 + [e(3a^4+b^4+c^4-2a^2b^2) - 2a^2d(b^2-c^2)]^2}}{3de(d+e)(a^4+b^4+c^4)}. \tag{34}$$

$$m_s = m_z \frac{\sqrt{c^2[a^2(d+e) + b^2e]^2 + b^2(a^2d - c^2e)^2 + a^2[c^2(d+e) + b^2d]^2}}{\sqrt{2}[a^2c^2(d+e)^2 + b^2(a^2d^2 + c^2e^2)]}, \tag{35}$$

$$m_p = m_z \sqrt{\frac{a^2d^2 + c^2e^2}{2[a^2c^2(d+e)^2 + b^2(a^2d^2 + c^2e^2)]}}, \tag{36}$$

$$m_q = m_z \frac{\sqrt{2\{[d^2(a^4+b^4+b^2c^2) + c^2e^2(a^2-b^2)]^2 + [d^2(a^4+c^4+b^2c^2) - e^2(a^4+c^4+a^2b^2)]^2 + [e^2(b^4+c^4+a^2b^2) - a^2d^2(b^2-c^2)]^2\} + [d^2(a^4+b^4+3c^4-2b^2c^2) - 2c^2e^2(a^2-b^2)]^2 + [(a^4+3b^4+c^4)(d^2-e^2) + 2b^2(a^2e^2 - c^2d^2)]^2 + [e^2(3a^4+b^4+c^4-2a^2b^2) + 2a^2d^2(b^2-c^2)]^2}}{3de(d+e)(a^4+b^4+c^4)}. \tag{37}$$

Let us derive expressions for RMSE of k_h and k_v (m_{k_h} and m_{k_v}, respectively) with the equation (29). Equations (1 and 2) should be tested to determine m_{k_h} and m_{k_v}, although some simplified expressions of k_h and k_v are common in the literature (e.g. Pennock *et al.* 1987, Zevenbergen and Thorne 1987). However, equations (1 and 2) most closely correspond to the physical and mathematical theory of surface in gravity (Shary 1991, 1995). As measured arguments, we use r, t, s, p and q calculated by the method developed (equations (24–28)). Formulae for m_{k_h} and m_{k_v} are developed in

a manner like m_r, m_t, m_s, m_p and m_q (equations (33–37)) were derived:

$$m_{kh} = \sqrt{\left(\frac{\partial k_h}{\partial r}\right)_0^2 m_r^2 + \left(\frac{\partial k_h}{\partial t}\right)_0^2 m_t^2 + \left(\frac{\partial k_h}{\partial s}\right)_0^2 m_s^2 + \left(\frac{\partial k_h}{\partial p}\right)_0^2 m_p^2 + \left(\frac{\partial k_h}{\partial q}\right)_0^2 m_q^2} = \ldots$$

$$\ldots = \frac{1}{p^2+q^2}\sqrt{\frac{1}{1+p^2+q^2}\left\{q^4 m_r^2 + 4p^2q^2m_s^2 + p^4 m_t^2 + 4[(qs-pt)^2 m_p^2 + (ps-qr)^2 m_q^2] + \right.}$$

$$\left. + \frac{q^2r-2pqs+p^2t}{(p^2+q^2)(1+p^2+q^2)}\left[\frac{(q^2r-2pqs+p^2t)[2.25(p^2+q^2)^2+3(p^2+q^2)+1](p^2m_p^2+q^2m_q^2)}{(p^2+q^2)(1+p^2+q^2)} + \right.\right.$$

$$\left.\left. + (3p^2+3q^2+2)[p(qs-pt)m_p^2 + q(ps-qr)m_q^2]\right]\right\}. \tag{38}$$

$$m_{kv} = \sqrt{\left(\frac{\partial k_v}{\partial r}\right)_0^2 m_r^2 + \left(\frac{\partial k_v}{\partial t}\right)_0^2 m_t^2 + \left(\frac{\partial k_v}{\partial s}\right)_0^2 m_s^2 + \left(\frac{\partial k_v}{\partial p}\right)_0^2 m_p^2 + \left(\frac{\partial k_v}{\partial q}\right)_0^2 m_q^2} = \ldots$$

$$\ldots = \frac{1}{p^2+q^2}\sqrt{\frac{1}{(1+p^2+q^2)^3}\left\{p^4 m_r^2 + 4p^2q^2m_s^2 + q^4 m_t^2 + 4[(qs+pr)^2 m_p^2 + (ps+qt)^2 m_q^2] + \right.}$$

$$\left. + \frac{p^2r+2pqs+q^2t}{(p^2+q^2)(1+p^2+q^2)}\left[\frac{(p^2r+2pqs+q^2t)[6.25(p^2+q^2)+5(p^2+q^2)+1](p^2m_p^2+q^2m_q^2)}{(p^2+q^2)(1+p^2+q^2)} - \right.\right.$$

$$\left.\left. - (5p^2+5q^2+2)[p(qs+pr)m_p^2 + q(ps+qt)m_q^2]\right]\right\}. \tag{39}$$

4. Method testing

4.1. *Study area*

The study area is situated in Central Eurasia (figure 2). The area lies within five 6° longitude zones and measures 30° by 20°. The study area is marked by a diversity of relief (figure 3 (*a*)) and tectonics (figure 3 (*b*)). The tectonic structure of the study area is complicated by many faults (Solovyev 1977, Suvorov 1997 a, 1977 b, Trifonov *et al.* 1983, Koronovsky 1984). North and northwest-striking faults are dominant. Some east and northeast-striking faults are also observed (figure 3 (*b*)). Generally, the topography depends directly on the tectonic structure within the area (Meshcheryakov 1972, Koronovsky 1984).

The central and southern parts of the study area are occupied by the Turan lowland (figure 3 (*a*)) relating to the Turan Epipalaeozoic plate (figure 3 (*b*)). There are marine, alluvial, arid destructional and accumulative plains (elevations are 50–200 m), plateaus (elevations are 300–400 m), depressions (depths are down to −132 m), and inselbergs (elevations are up to 1000 m). The Kazakh hummocky terrain is situated to the north-east of the Turan lowland (figure 3 (*a*)) within the Central Kazakhstan Caledonian and the Dzhungar–Balkhash Hercynian folding zones (figure 3 (*b*)). There is a high rolling plain with numerous hills (elevations are 300–500 m) and some low mountains (elevations are up to 1566 m). The South Urals are located north of the Turan lowland (figure 3 (*a*)). They are epiplatformian middle mountains (elevations are up to 1640 m) corresponding to the Ural Hercynian folding zone (figure 3 (*b*)). The South Urals consist of a main watershed ridge and some

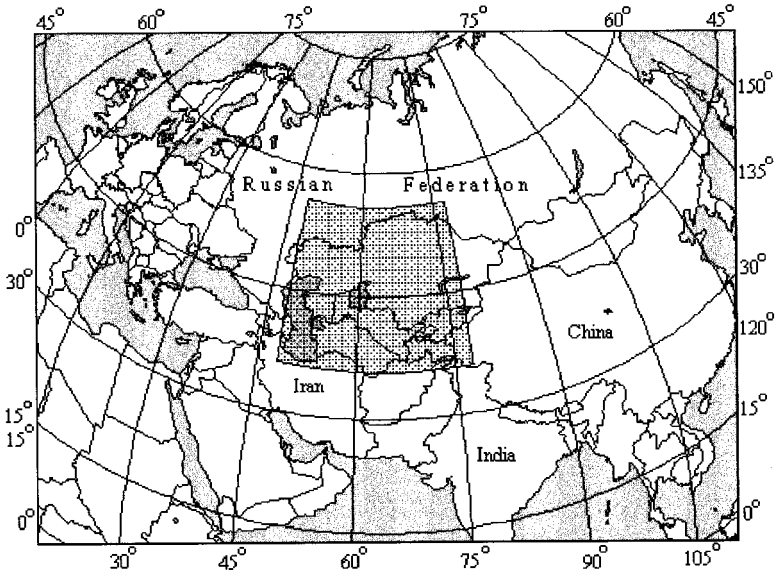

Figure 2. Geographical location of the study area (between 36° and 56° N, and 48° and 78° E).

lateral ridges divided by broad depressions. The West Siberian plain is located east of the South Urals (figure 3 (*a*)). This is an inclined plain (elevations are up to 300 m) corresponding to the West Siberian Epipalaeozoic plate (figure 3 (*b*)). The Obshchy Syrt plateau and the Bugulma–Belebey upland (elevations are up to 400 m) are situated to the west of the South Urals (figure 3 (*a*)). These terrains relate to the south-east edge of the East European Precambrian platform (figure 3 (*b*)).

There are the Caspian lowland and the Caspian sea depression in the west of the study area (figure 3 (*a*)). The Caspian lowland (elevations range from −28 m to 100 m) relates to the East European Precambrian platform (figure 3 (*b*)). The northern part of the Caspian depression (depths are down to −790 m) corresponds to the junction of the Turan and the Scythian Epipalaeozoic plates. The South Caspian abyssal depression (depths are down to −1025 m) lacks the granite layer.

Epiplatformian mountains of the West Tien Shan and the Gissaro-Alai are located south of the Kazakh hummocky terrain (figure 3 (*a*)). Generally, the Gissaro-Alai have an alpine type of relief (elevations are up to 5621 m). The Tien Shan consist of three near-east-striking block ridges (elevations are up to 7439 m) divided by inter-mountain depressions. These territories correspond to the North Tien Shan Caledonian and the South Tien Shan Hercynian folding zones (figure 3 (*b*)). In the south-west of the study area there are eastern extremities of the Great Caucasus ridges (elevations are up to 3000 m), some ridges of the Elburz (elevations are up to 4000 m), and the Kopetdag mountains (elevations are up to 3117 m) (figure 3 (*a*)). These systems relate to Alpine folding zones of the Mediterranean geosynclinal belt (figure 3 (*b*)). In the south-east of the study area are the north-eastern ridges of the Hindu Kush, the Pamir mountainous land, north-western extremities of the Karakorum and the Kun Lun ridges, and the western part of the Kashgar plain (figure 3 (*a*)). The Hindu Kush are alpine mountains (elevations are up to 7690 m). The eastern and western Pamirs involve alpine ridges (elevations are up to 7497 m),

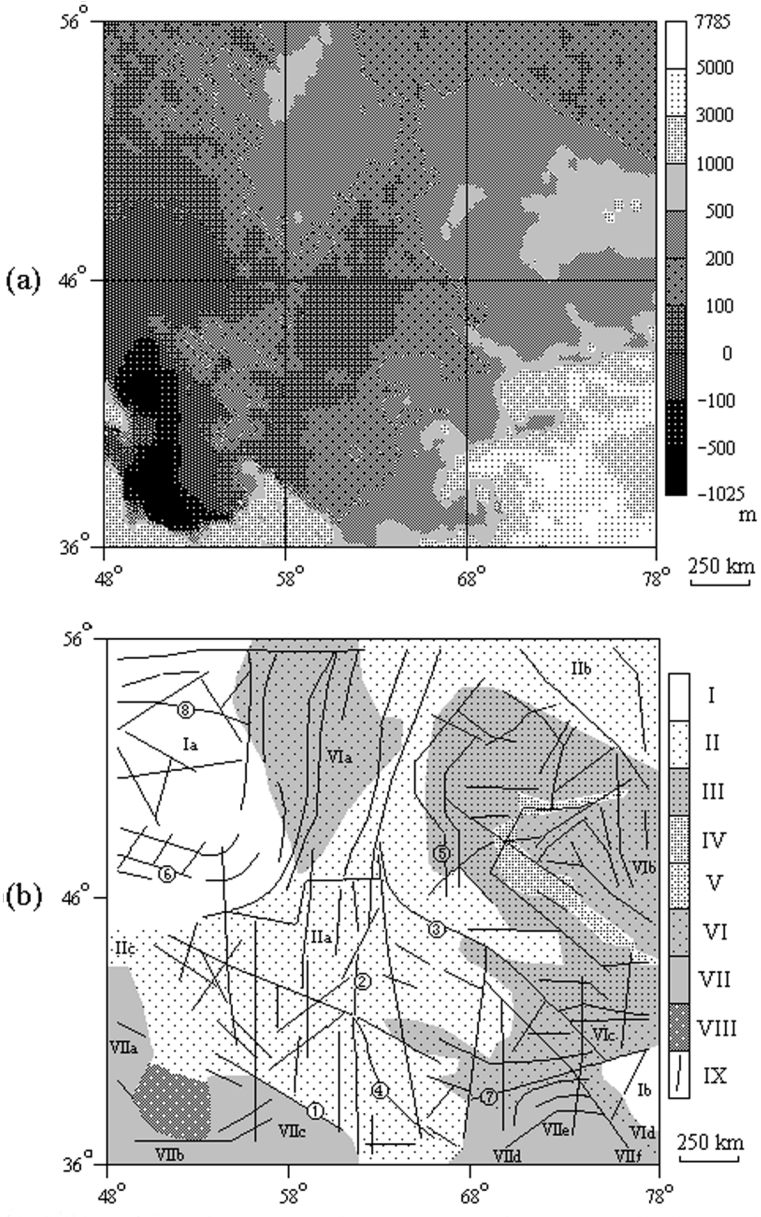

Figure 3. The study area: (*a*) elevation map, (*b*) generalised tectonic scheme (Solovyev 1977, Suvorov 1977 a, 1977 b, Trifonov *et al.* 1983, Koronovsky 1984): I Precambrian platform and massif: Ia East European platform, Ib Tarim massif; II Epipalaeozoic plates: IIa Turan plate, IIb West Siberian plate, IIc Scythian plate; III Central Kazakhstan–North Tien Shan Caledonian folding zone; IV Kazakhstan Devonian volcanic belt; V Ili–Balkhash Carboniferous–Permian volcanic belt; VI Hercynian folding zones: VIa Ural zone, VIb Dzhungar–Balkhash zone, VIc South Tien Shan zone, VId Kun Lun zone; VII Alpine folding zones: VIIa Caucasus zone, VIIb Elburz zone, VIIc Kopetdag zone, VIId Hindu Kush zone, VIIe Pamir zone, VIIf Karakorum zone; VIII South Caspian abyssal depression; IX faults: 1 Kopetdag strike-slip fault and thrust, 2 fault, 3 Talas-Fergana oblique-slip fault, 4 Amudarya dip-slip fault, 5 West Ulutau thrust, 6 Guryev fault, 7 Vakhsh thrust, 8 Samara-Toksk dislocation megazone.

while the central Pamirs consist of weathered ridges (elevations are up to 6000 m) and flat valleys and depressions (elevations are 3500–4500 m). The Karakorum have alpine landforms, with the highest point of the study area (7785 m). The Hindu Kush, the Pamirs and the Karakorum relate to Alpine folding zones of the Mediterranean geosynclinal belt, while the Kun Lun relates to a Hercynian folding zone (figure 3 (*b*)). The Kashgar plain has elevations of about 1300 m, it corresponds to the Tarim Precambrian platformian massif (figure 3 (*b*)).

4.2. *Materials and methods*

To test the method developed we compiled a spheroidal trapezoidal-spaced DEM of the study area using 25 sheets of 1:1 000 000 scaled topographic map (General Headquarters 1960–1967, Central Board of Geodesy and Cartography 1962–1969). We digitised elevation values in nodes of the regular grid with 0.5° mesh. As a rule, elevation values were interpolated manually using contours. The DEM obtained includes 2501 points.

Results of k_h and k_v calculation and mapping essentially depend on DEM grid size as demonstrated by some experiments (Evans 1980, Florinsky 1991, Kuryakova 1996) and an analysis of equations (24–28). Upon increasing DEM grid size, one can produce more generalised versions of k_h and k_v maps. To study this effect we obtained k_h and k_v models by the method developed using two grid sizes: 0.5° (figures 4 (*a*) and 5 (*a*)) and 1° (figures 4 (*b*) and 5(*b*)). Also, we derived m_{k_h} and m_{k_v} models with these grid sizes (figures 4 (*c*), 4 (*d*), 5 (*c*) and 5 (*d*)). Digital models of k_h, k_v, m_{k_h} and m_{k_v} calculated with the grid size of 0.5° include 2301 points, while related models calculated with the grid size of 1° include 551 points.

As *a*, *b*, *c*, *d* and *e* we used values of parallel and meridian arc lengths relating to the Krasovsky ellipsoid (Bugaevsky and Vakhrameyeva 1992). The length of 0.5° parallel arc ranges from 45 083 m on 36° N to 31 197 m on 56° N, while the length of 0.5° meridian arc ranges between 55 488 m on 36° N and 55 679 m on 56° N.

In the DEM compilation, we used interpolation of contours (see above), so the equation (31) can be applied to estimate values of m_z. We set the factor $B=0.25$ as a median value from the proposed ones (§3). A contour interval Δz varies from 25 m to 200 m with geomorphic conditions (table 1) within the maps used. Therefore, for different parts of the DEM we applied different values of m_z (table 1) in calculation of m_r, m_t, m_s, m_p and m_q (equations (33–37)).

For revealing topographically expressed faults it is necessary (*a*) to calculate k_h and k_v by DEM processing, (*b*) to stratify k_h and k_v values into two levels with respect to the zero, and (*c*) to map k_h and k_v. Lineaments revealed on k_h maps indicate faults formed mostly by horizontal tectonic motions (i.e. strike-slip faults). Lineaments recognised by k_v mapping correspond to faults formed mainly by vertical motions (i.e. dip-slip and reverse faults) and thrusting. Lineaments recorded on both k_h and k_v maps indicate, as a rule, oblique-slip and gaping faults. For non-inverted relief, one can compare elevations on one and the other sides of a lineament on a k_v map to determine the direction of a vertical displacement. The detailed justification, description and limitations of the topographic method of fault morphology recognition can be found elsewhere (Florinsky 1996).

We compiled the map of revealed and morphologically classified faults (figure 6) by a visual analysis of the k_h and k_v maps obtained with the grid size of 0.5° (figures 4 (*a*) and 5 (*a*)). Generally, to compile the fault map (figure 6) we drew median lines of lineaments recorded on the k_h and k_v maps (figures 4 (*a*) and 5 (*a*)). We did

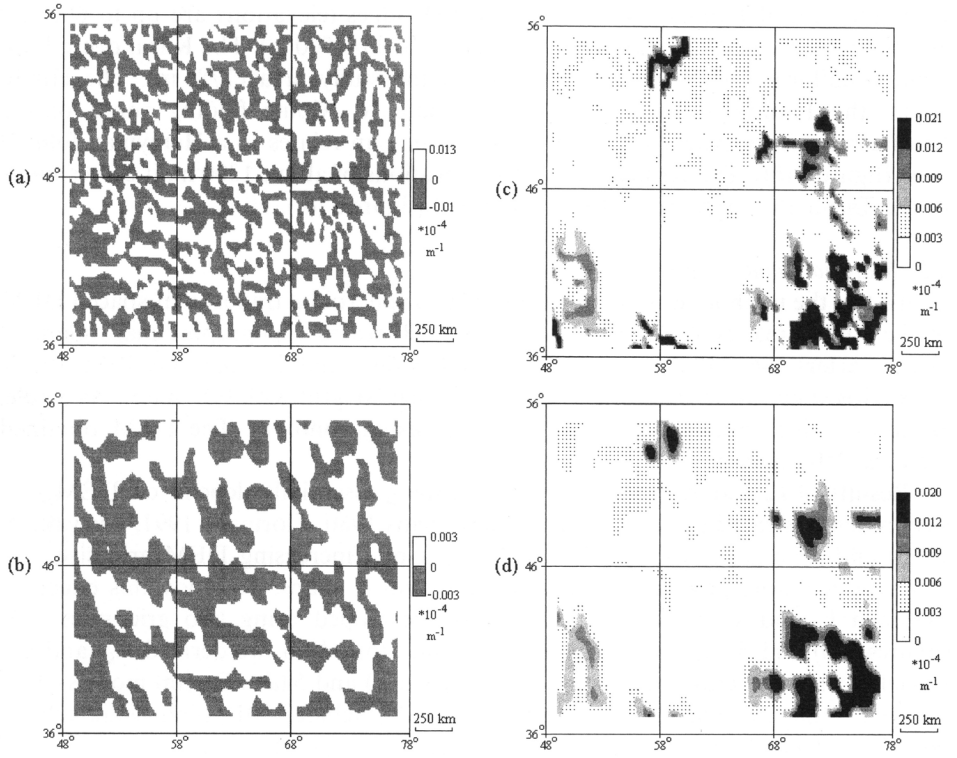

Figure 4. The study area: (*a*) k_h calculated for the grid size of 0.5°, (*b*) k_h calculated for the grid size of 1°, (*c*) m_{k_h} calculated for the grid size of 0.5°, (*d*) m_{k_h} calculated for the grid size of 1°.

not analyse the k_h and k_v maps with the resolution of 1° (figures 4 (*b*) and 5 (*b*)) due to their poor informative capacity (§5). To estimate the efficiency of the method we carried out a visual comparative analysis of the fault map obtained (figure 6) and some factual geological data (Solovyev 1977, Suvorov 1977 a, 1977 b, Trifonov *et al.* 1983, Koronovsky 1984).

We did not perform a correlation analysis of the fault map obtained (figure 6) and published data as the latter have dissimilar precision, scales, and are different from one another. Some faults are revealed by all authors, others are included only on a single map. Sometimes the same fault is presented with different lengths or strikes on different maps. At the same time, we cannot use only a single published map because the data from different maps complement each other.

It is our intention neither to improve reported limitations of the technique for fault morphology recognition (Florinsky 1996), nor to perform geological investigation of the study area. We use these examples to test the method developed, therefore we describe geological aspects only briefly.

Software for the calculation of topographic variables with spheroidal trapezoidal-spaced DEMs was developed by P. V. Kozlov (ZAO 'IC Protek', Moscow, Russia) using Borland Delphi, Version 3.0. Mapping of z, k_h, m_{k_h}, k_v and m_{k_v} (figures 3 (*a*), 4 and 5) was carried out by the software LANDLORD 2.0 (Florinsky *et al.* 1995). We applied an equidistant cylindrical projection to map topographic and geological data (figures 3, 4, 5 and 6): 46° N was used as the parallel of no distortion.

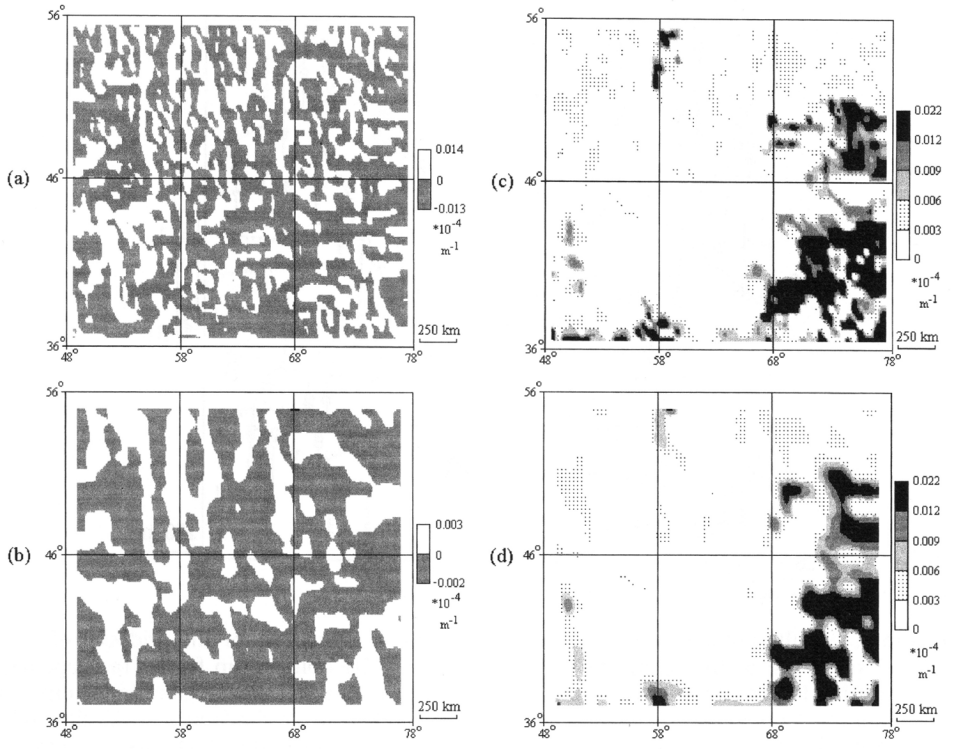

Figure 5. The study area: (*a*) k_v calculated for the grid size of 0.5°, (*b*) k_v calculated for the grid size of 1°, (*c*) (*d*) m_{k_v} calculated for the grid size of 0.5°, (*d*) (*d*) m_{k_v} calculated for the grid size of 1°.

Table 1. Relationship between elevation ranges, contour intervals and m_z for the study area.

z, m	Δz, m	m_z, m
from −950 till −100	100	25
from −100 till −50	50	12.5
from −50 till 400	25*	6.25
from 400 till 1000	100	25
from 1000 till 7200	200	50

*Taking into consideration additional contours.

5. Results and discussion

Mapping of k_h and k_v obtained with the DEM resolution of 0.5° allows us to reveal many lineaments of different directions and sizes (figures 4(*a*) and 5(*a*)). We interpret lineaments recorded on the k_h map (figure 4(*a*)) as strike-slip faults (figure 6). Structures recorded on the k_v map (figure 5(*a*)) are interpreted as dip-slip faults and thrusts (figure 6). Lineaments revealed on both k_h and k_v maps (figures 4(*a*) and 5(*a*)) are interpreted as oblique-slip faults (figure 6).

Most of the faults revealed are near-north and near-northwest-striking ones (figure 6) much as most of the observed faults (figure 3(*b*)). A visual comparative analysis of the fault map obtained (figure 6) and factual geological data (Solovyev 1977, Suvorov 1977a, 1977b, Trifonov *et al.* 1983, Koronovsky 1984) made it apparent

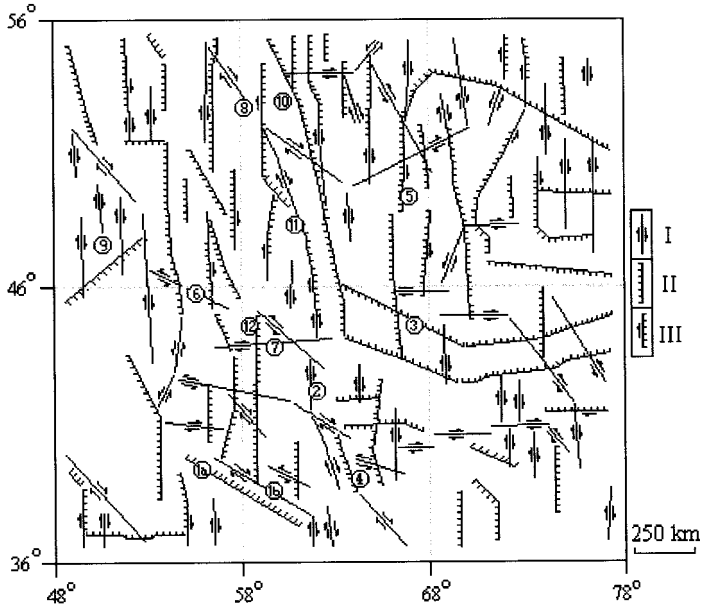

Figure 6. Faults revealed with the maps of k_h and k_v calculated for the grid size of 0.5°; I strike-slip faults, II dip-slip faults and thrusts, III oblique-slip faults: 1a Kopetdag thrust, 1b Kopetdag strike-slip fault, 2 strike-slip fault, 3 Talas-Fergana hinge dip-slip fault, 4 Amudarya dip-slip fault, 5 oblique-slip fault, 6 strike-slip fault, 7 strike-slip fault, 8 dip-slip fault, 9 complex of strike-slip faults, 10 complex of dip-slip faults, 11 complicated fault, 12 hinge dip-slip fault.

that a portion of the revealed faults is strongly correlated with familiar ones. For instance, there is the Kopetdag thrust and strike-slip fault, and fault '2' (figures 3(*b*) and 6). A portion of the revealed faults partially fits familiar structures (e.g. the Tales-Fergana and the Amudarya dip-slip faults—figures 3(*b*) and 6). Some revealed faults are extentions of familiar ones. For example, oblique-slip fault '5' is an extension of the West Ulutau thrust, and strike-slip fault '6' is an extension of the Guryev fault (figures 3(*b*) and 6). A portion of the revealed faults does not correlate with faults mapped by Solovyev (1977), Suvorov (1977a, 1977b), Trifonov *et al.* (1983) and Koronovsky (1984). Among these are strike-slip fault '7' and dip-slip fault '8' (figure 6). Their origin is the subject of a specific study. Also, not all the familar faults are revealed, such as the Vakhsh thrust and the Samara-Toksk dislocation megazone (figure 3(*b*)). This can be the result of using the single grid size for fault revealing. To recognise all the topographically expressed faults one should apply a set of k_h and k_v maps obtained with a range of grid sizes (Florinsky 1996). Besides, relief cannot express some faults.

The fault map obtained displays a complicated spatial distribution of structures (figure 6). Strike-slip, dip-slip and thrusts unite into complexes (e.g. complexes '9' and '10'—figure 6). As a rule, strike-slip faults stretch across dip-slip ones. Some complicated faults include dip-slip, strike-slip and oblique-slip offsets (e.g fault '11—figure 6). Also, some hinge dip-slip faults are revealed, such as the Talas-Fergana fault and fault '12' (figure 6). These tendencies of fault distribution were also found for other regions by the topographic method of fault revealing using square-spaced DEMs and the Evans method (Florinsky *et al.* 1995, Florinsky 1996). The results

obtained demonstrate that the method developed actually works with respect to fault revealing in regions marked by complicated topographic and tectonic conditions.

Using the grid size of 1°, we obtained generalised versions of k_h and k_v maps (figures 4(*b*) and 5(*b*)). Narrow zones of flow divergence ($k_h > 0$) and convergence ($k_h < 0$) (figure 4(*a*)) transformed to corresponding wide strips (figure 4(*b*)). In a similar manner, narrow zones of relative flow acceleration ($k_v > 0$) and deceleration ($k_v < 0$) (figure 5(*a*)) transformed to corresponding wide areas (figure 5(*b*)). Notice that maximal values of k_h and k_v obtained with the grid size of 1° (figures 4(*b*) and 5(*b*)) are one order of magnitude smaller than maximal values of these variables obtained with the grid size of 0.5° (figures 4(*a*) and 5(*a*)). With increasing DEM grid size, analogous trends for slope gradient, k_h, k_v, mean and total landsurface curvatures were observed before (Evans 1980, Chang and Tsai 1991, Florinsky 1991, Kuryakova 1996).

Notice that k_h and k_v maps obtained with the grid size of 1° (figures 4(*b*) and 5(*b*)) are too generalised: they are marked by poor informative capacity. In geomorphic and geological investigations, DEM grid size depends on the typical size of landforms or geological structures of interest (Evans 1972, Florinsky 1996). However, for each DEM one can find experimentally a specific range of grid sizes to reach a compromise between amount of information and readability and interpretability of the k_h and k_v maps (Florinsky 1991, Kuryakova 1996). The DEM resolution, geomorphic conditions, size of a territory, and scale of k_h and k_v maps dictate this grid size range. For the study area (§4.1) and the DEM used (§4.2, figure 3(*a*)) the grid size of 0.5° is among the range of proper grid sizes, while the grid size of 1° is outside this range. This is demonstrated by the information-poor maps of k_h and k_v (figures 4(*b*) and 5(*b*)) relating to the latter resolution. This resolution may be appropriate for territories measuring 50° by 50° and more, and for mapping at scales of 1 : 50 000 000 and smaller.

The spatial distribution of m_{k_h} and m_{k_v} obtained with grid size of 0.5° (figures 4(*c*) and 5(*c*) depends directly on the m_z distribution. Indeed, high values of m_{k_h} and m_{k_v} are, as a rule, located within mountainous regions marked by high values of m_z due to large contour intervals (table 1, §4.2). Within these areas values of m_{k_h} and m_{k_v} exceed maximal values of k_h and k_v, respectively. However, this does not mean that k_h and k_v maps (figures 4(*a*) and 5(*a*)) are invalid there. This is because RMSE is a *statistical* property of a function F, that is, m_F indicates a *probability* of error rather than the mandatory existence of error. Within zones marked by high values of m_{k_h} and m_{k_v} one has to interpret data on k_h and k_v with scepticism or, better still, to recompile these DEM portions (Hunter and Goodchild 1995, Florinsky 1998a) using the same grid size but more precise maps (with smaller contour interval and thus smaller m_z). Therefore, it is wise to digitise contours of middle-scaled topographic maps (e.g., 1 : 200 000) if one studies a mountainous region using DTM resolution of about 0.5° and more.

Using the grid size of 1°, we obtained generalised versions of m_{k_h} and m_{k_v} maps (figures 4(*d*) and 5(*d*)). In this case, the trend of spatial distribution of m_{k_h} and m_{k_v} is identical to that for the grid size of 0.5° (figures 4(*c*) and 5(*c*)). Maximal values of m_{k_h} and m_{k_v} are much the same for DEM resolution of both 0.5° (figures 4(*c*) and 5(*c*)) and 1° (figures 4(*d*) and 5(*d*)). It is notably that areas with high values of m_{k_h} (figures 4(*c*) and 4(*d*)) are marked by low values of m_{k_v} (figures 5(*c*) and 5(*d*)), and *vice versa*. We suppose that this property of the m_{k_h} and m_{k_v} functions (equations (38 and (39)) may be observed in any other areas.

The following question arises: how much difference does the method developed make in r, t, s, p, q, k_h and k_v calculation compared with the Evans method? This comparison can be done only if we can apply both the Evans method and the method proposed to a common DEM, that is, nodes of a plane square grid coincide with nodes of a spheroidal trapezoidal grid. For example, Guzzetti and Reichenbach (1994) used a square-spaced DEM of Italy marked by the resolution of 7.7″ of latitude and 10″ of longitude, that is, $w \approx 230$ m. In this case $a = b = c = d = e = w$, so equations (24–28) reduce to equations (5–9). Therefore, application of both the Evans method and the method developed gives identical results: a test is not needed. Along similar lines, equations (33–39) reduce to related formulae of m_r, m_t, m_s, m_p, m_q, m_{k_h} and m_{k_v} for the Evans method (Florinsky 1998a) if $a = b = c = d = e = w$.

The method developed opens up new avenues for carrying out some 'conventional' raster operations directly on geographical co-ordinates. For example, equations (27 and 28) can be applied to derive slope gradient and aspect (Evans 1972, 1980, Shary 1991) and reflectance (Horn 1981), since the latest is used in regional and continental works (Moore and Simpson 1983, Edwards and Davis 1994, Guzzetti and Reichenbach 1994). Also, the method can be used to derive variables of imaginary surfaces, such as a mean curvature of a 'surface' of a velocity of the modern vertical movements of the Earth's crust (Grachev *et al.* 1988).

Besides, the method can be employed to treat available spheroidal trapezoidal-spaced DEMs, for instance, the 5′-spaced global DEM, ETOPO5 (NOAA 1988), and the 56.25″-spaced DEM of Mars (Batson and Eliason 1995). Although one may interpolate DEMs of this sort into square-shaped ones (e.g. Moore and Simpson 1983), errors can occur in the resulting DEMs (Schut 1976). Moreover, operational difficulties may arise for a sizeable territory under study (§1). So, there are good reasons to process these DEMs without transformation into square-spaced ones.

There is a further reason to use spheroidal trapezoidal-spaced DEMs and the method developed. Geological investigations can involve a combined analysis of geological, geophysical and topographic data (Ollier 1981, Moore and Simpson 1983, Poletaev *et al.* 1991, McMahon and North 1993). Generally, geophysical data are available with spheroidal trapezoidal grids. In addition, the spherical co-ordinate system is at times used to prevent projection distortions in geological experiments Besprozvanny *et al.* 1994). Utilisation of DTMs given by the same grid type can simplify and improve comparison of topographic, geophysical and geological data, since one can omit ancillary steps of projection transformation and interpolation.

In closing we should stress again that we designed the method for the case that the Earth's shape is ignored, that is, for DEM grid meshes of no more than 225 km. The Earth's sphericity has to be taken into account if one should derive k_h and k_v from a DEM with greater grid mesh. However, development of a related method is the subject of another study.

6. Conclusions

1. DEMs given by spheroidal trapezoidal grids are more appropriate for large regional, sub-continental, continental and global geological and soil studies than square-spaced DEMs.
2. We developed the method for derivation of topographic variables, specifically k_h and k_v, from DEMs given by spheroidal trapezoidal grids. Equations for calculation of r, t, s, p and q with DEMs of this sort were derived. Also,

formulae for estimation of m_r, m_t, m_s, m_p, m_q, m_{k_h} and m_{k_v} were produced. We designed the method for the case that the Earth's shape is ignored, that is, for DEM grid sizes of no more than 225 km.

3. We tested the method by the example of fault recognition. A comparative analysis of the test results and factual geological data demonstrates that the method actually works in regions marked by complicated topographic and tectonic conditions.
4. Upon increasing the DEM grid size, one can produce generalised maps of k_h and k_v. For each DEM, one can find a specific range of grid sizes to reach a compromise between the amount of information and the readability and interpretability of k_h and k_v maps.
5. Spatial distribution of m_{k_h} and m_{k_v} depends directly on spatial distribution of m_z. Areas with high values of m_{k_h} are marked by low values of m_{k_v}, and *vice versa*, areas with high values of m_{k_v} are marked by low values of m_{k_h}. Data on m_{k_h} and m_{k_v} should be applied to control and improve utilisation of k_h and k_v in geological studies.
6. The method developed opens up new avenues for carrying out some 'conventional' raster operations directly on geographical co-ordinates.

Acknowledgments

The author performed the work without a financial support from government and private funds. The author is grateful to P. V. Kozlov (ZAO 'IC Protek', Moscow, Russia) for development of a software, Z. F. Povetukhina (Institute of Soil Science and Photosynthesis, Russian Academy of Sciences, Pushchino, Russia) for provision of maps, and anonymous referees for useful criticism.

References

Aandahl, A. R., 1948, The characterization of slope positions and their influence on the total nitrogen content of a few virgin soils of western Iowa. *Soil Science Society of America Proceedings*, **13,** 449–454.

Anisimov, I. G., Bordunov, A. A., Deeva, N. F., Kamalov, L. F., Muratova, V. S., Peido, L. P., Povetukhina, Z. F., Stepanov, G. N., Ushakova, T. P., Khakimov, F. I., and Chembarisov, E. I., 1977, Technique for compilation of the series of middle-scaled thematical maps of 'Natural and Reclamation Estimation of the Middle Region of the USSR'. In *Estimation of Natural and Reclamation Conditions and Prediction of Their Changes (Exemplified from the Middle Asia)*, edited by I. N. Stepanov (Pushchino: Biological Research Centre Press), pp. 23–93 (in Russian).

Batson, R. M., and Eliason, E. M., 1995, Digital maps of Mars. *Photogrammetric Engineering and Remote Sensing*, **61,** 1499–1507.

Besprozvanny, P. A., Borodzich, E. V., and Bush, V. A., 1994, On revealing of an order for a planetary lineament network by the results of numerical testing. *Physica Zemli*, **2,** 57–66 (in Russian).

Bjerhammar, A., 1973, *Theory of Errors and Generalized Matrix Inverses* (Amsterdam: Elsevier).

Bobir, N. Ya., Lobanov, A. N., and Fedoruk, G. D., 1974, *Photogrammetry* (Moscow: Nedra) (in Russian).

Bronstein, I. N., and Semendyaev, K. A., 1956, *Mathematical Handbook for Engineers and Students*, 6th edition (Moscow: State Press for Technical and Theoretical Literature) (in Russian).

Bugaevsky, L. M., and Vakhrameyeva, L. A., 1992, *Cartographic Projections: A Handbook* (Moscow: Nedra) (in Russian).

Burrough, P. A., 1986, *Principles of Geographical Information Systems for Land Resources Assessment* (Oxford: Clarendon Press).

Burt, T. P., and Butcher, D. P., 1985, Topographic controls of soil moisture distribution. *Journal of Soil Science*, **36,** 469–486.

Carey, S. W., 1988, *Theories of the Earth and Universe. A History of Dogma in the Earth Sciences* (Stanford: Stanford University Press).

Central Board of Geodesy and Cartography, 1962–1969, *Topographic Map, scale 1:1000000. Sheets: K–39 (Baku), K–40 (Nukus), K–41 (Urgench), K–42 (Tashkent), K–43 (Alma-Ata–Frunze), L–39 (Astrakhan), L–40 (Chelker), L–41 (Kzyl-Orda), L–42 (Dzhezkazgan), L–43 (Balkhash), M–39 (Uralsk), M–40 (Orenburg), M–41 (Turgai), M–42 (Tselinograd), M–43 (Karaganda), N–39 (Kazan–Kuibyshev), N–40 (Ufa–Magnitogorsk), N–41 (Chelyabinsk), N–42 (Petropavlovsk), N–43 (Omsk)* (Moscow: Central Board of Geodesy and Cartography) (in Russian).

Chang, K.-T., and Tsai, B.-W., 1991, The effect of DEM resolution on slope and aspect mapping. *Cartography and Geographical Information Systems*, **18,** 69–77.

Dikau, R., 1988, Case studies in the development of derived geomorphic maps. *Geologiches Jahrbuch*, **A 104,** 329–338.

Edwards, K., and Davis, P. A., 1994, The use of intensity-hue-saturation transformation for producing color shaded-relief images. *Photogrammetric Engineering and Remote Sensing*, **60,** 1369–1374.

Evans, I. S., 1972, General geomorphometry, derivations of altitude, and descriptive statistics. In *Spatial Analysis in Geomorphology*, edited by R. J. Chorley (London: Methuen), pp. 17–90.

Evans, I. S., 1979, An integrated system of terrain analysis and slope mapping. Final report on grant DA-ERO-591-73-G0040 (Durham: University of Durham).

Evans, I. S., 1980, An integrated system of terrain analysis and slope mapping. *Zeitschrift für Geomorphologie*, Suppl. Bd. **36,** 274–295.

Evans, I. S., 1987, The morphometry of specific landforms. In *International Geomorphology 1986: Proceedings of the First International Conference on Geomorphology, Manchester, 1986. Pt. 2* (Chichester: John Wiley and Sons), pp. 105–124.

Felicisimo, A. M., 1994, *Modelos Digitales del Terreno. Introducción y Aplicaciones en las Ciencias Ambientales* (Oviedo: Pentalfa Ediciones).

Feranec, J., Kolar, J., and Krcho, J., 1991, Mapping of the surface water logging intensity of the soils by applying Landsat TM data and complex digital terrain model. *Bulletin du Comite Francais de Cartographie*, **127–128,** 154–157.

Florinsky, I. V., 1991, *Map Generalisation: a Brief Review of the Problem* (Puschchino: Pushchino Research Centre Press) (in Russian).

Florinsky, I. V., 1992, *Recognition of Lineaments and Ring Structures: Quantitative Topographic Techniques* (Pushchino: Pushchino Research Centre Press) (in Russian, with English abstract).

Florinsky, I. V., 1996, Quantitative topographic method of fault morphology recognition. *Geomorphology*, **16,** 103–119.

Florinsky, I. V., 1998a, Accuracy of local topographic variables derived from digital elevation models. *International Journal of Geographical Information Science*, **12,** 47–61.

Florinsky, I. V., 1998b, Combined analysis of digital terrain models and remotely sensed data in landscape investigations. *Progress in Physical Geography*, **22,** 33–60.

Florinsky, I. V., and Kuryakova, G. A., 1996, Influence of topography on some vegetation cover properties. *Catena*, **27,** 123–141.

Florinsky, I. V., Grokhlina, T. I., and Mikhailova, N. L., 1995, Landlord 2.0: The software of analysis and mapping of geometrical characteristics of relief. *Geodesiya i Cartographiya*, **5,** 46–51 (in Russian).

Franklin, S. E., 1987, Geomorphometric processing of digital elevation models. *Computers and Geosciences*, **13,** 603–609.

Gaidaev, P. A., and Bolshakov, V. D., 1969, *Theory of Mathematical Processing of Geodetic Measurements* (Moscow: Nedra) (in Russian).

Geiger, R., 1966, *The Climate near the Ground. Translation by Scripta Technica from the 4th German edition 2nd print* (Cambridge: Harvard University Press).

General Headquarters, 1960–1967, *Topographic Map, scale 1:1000000. Sheets: J–39 (the south part of the Caspian Sea), J–40 (Ashkhabad), J–41 (Bukhara), J–42 (Dushanbe), J–43 (Pamir)* (Moscow: General Headquarters) (in Russian).

GERRARD, A. J., 1981, *Soils and Landforms. An Integration of Geomorphology and Pedology* (London: George Allen and Unwin).

GESSLER, P. E., MOORE, I. D., MCKENZIE, N. J., and RYAN, P. J., 1995, Soil-landscape modelling and spatial prediction of soil attributes. *International Journal of Geographical Information Systems*, **9,** 421–432.

GRACHEV, A. F., KALASHNIKOVA, I. V., and MAGNITSKY, V. A., 1988, Velocities of lithosphere straining and seismicity. *Doklady Academii Nauk SSSR*, **302,** 579–582 (in Russian).

GUZZETTI, F., and REICHENBACH, P., 1994, Towards a definition of topographic devisions for Italy. *Geomorphology*, **11,** 57–74.

HORN, B. K. P., 1981, Hill shading and the reflectance map. *Proceedings of the Institute of Electrical and Electronics Engineers*, **69,** 14–47.

HUNTER, G. J., and GOODCHILD, M. F., 1995, Dealing with error in spatial databases: a simple case study. *Photogrammetric Engineering and Remote Sensing*, **61,** 529–537.

KIRKBY, M. S., and CHORLEY, R. J., 1967, Throughflow, overland flow and erosion. *Bulletin of the International Association of Scientific Hydrology*, **12,** 5–21.

KORONOVSKY, N. V., 1984, *Brief Course of Regional Geology of the USSR*. 2nd edition (Moscow: Moscow State University Press) (in Russian).

KRCHO, J., 1973, Morphometric analysis of relief on the basis of geometric aspect of field theory. *Acta Geographica Universitatis Comenianae, Geographico-Physica*, **1,** 7–233.

KUMLER, M. P., 1994, An intensive comparison of triangulated irregular networks (TINs) and digital elevation models (DEMs). *Cartographica*, **31,** 1–99.

KURYAKOVA, G. A., 1996, Strategy for Investigation and Preparation of Initial Data for Biogeocoenosis Mapping with Digital Terrain Models: Abstract of Ph.D. Thesis (Moscow: Moscow State University of Geodesy and Cartography) (in Russian).

KURYAKOVA, G. A., and FLORINSKY, I. V., 1991, *The Analysis of Spatial Relations between Ring Structures, Topography and Soil Cover* (Pushchino: Pushchino Research Centre Press) (in Russian, with English abstract).

KVIETKAUSKAS, V., 1963–1964, Keturspalvis morfografinis zemelapis. In *Geografinis Metraštis VI–VII. Ledyninio Reljefo Morfogeneze ir Dabartiniai Egzogeninia Procesai*, edited by S. Tarvydas (Vilnius: Lietuvos TSR Geografine Draugija), pp. 87–107 (in Lithuanian, with German abtrast).

LANYON, L. E., and HALL, G. F., 1983, Land surface morphology: 2. Predicting potential landscape instability in eastern Ohio. *Soil Science*, **136,** 382–386.

LI, Z., 1994, A comparative study of the accuracy of digital terrain models (DTMs) based on various data models. *ISPRS Journal of Photogrammetry and Remote Sensing*, **49,** 2–11.

MARTZ, L. W., and DE JONG, E., 1987, Using Cesium-137 to assess the variability of net soil erosion and its association with topography in a Canadian Prairie landscape. *Catena*, **14,** 439–451.

MCMAHON, M. J., and NORTH, C. P., 1993, Three-dimensional integration of remotely sensed geological data: A methodology for petroleum exploration. *Photogrammetric Engineering and Remote Sensing*, **59,** 1251–1256.

MESHCHERYAKOV, YU. A., 1972, *Relief of the USSR* (Moscow: Mysl) (in Russian).

MILLER, C. L., and LEFLAMME, R. A., 1958, The digital terrain model—Theory and application. *Photogrammetric Engineering*, **24,** 433–442.

MODRINSKY, N. I., 1972, *Geodesy*. 3rd edition (Leningrad: Hydrometeoizdat) (in Russian).

MOORE, I. D., GRAYSON, R. B., and LADSON, A. R., 1991, Digital terrain modelling: A review of hydrological, geomorphological and biological applications. *Hydrological Processes*, **5,** 3–30.

MOORE, I. D., GESSLER, P. E., NIELSEN, G. A., and PETERSON, G. A., 1993, Soil attribute prediction using terrain analysis. *Soil Science Society of America Journal*, **57,** 443–452.

MOOR, R. F., and SIMPSON, C. J., 1983, Image analysis—A new aid in morphometric studies. In *Proceedings of the 17th International Symposium Remote Sensing of Environment, Ann Arbor, 9–13 May 1983*, **Vol. 3** (Ann Arbor: Environmental Research Institute of Michigan), pp. 991–1002.

NOAA, 1988, *Data Announcement 88-MGG-02, Digital Relief of the Surface of the Earth* (Boulder: NOAA, National Geophysical Data Center).

OLLIER, C., 1981, *Tectonics and Landforms* (London: Longman).

PENNOCK, D. J., ZEBARTH, B. J., and DE JONG, E., 1987, Landform classification and soil distribution in hummocky terrain, Saskatchewan, Canada. *Geoderma*, **40,** 297–315.

Poletaev, A. I., Kats, Ya. G., and Leonov, N. N., 1991, Revealing of active fault and lineament structures within the area of the Smolensk Nuclear Power Station by visual and automated analysis. In *Digital Processing of Videoinformation in Structural Geological and Siesmotectonic Investigations*, edited by B. N. Mozhaev (Leningrad: Aerogeologiya), pp. 42–55 (in Russian).

Pratt, W. K., 1978, *Digital Image Processing* (New York: John Wiley and Sons).

Salishchev, K. A., 1990, *Map Science*. 3rd edition (Moscow: Moscow State University Press) (in Russian).

Schut, G. H., 1976, Review of interpolation methods for digital terrain models. *The Canadian Surveyor*, **30,** 389–412.

Sharpnack, D. A., and Akin, G., 1969, An algorithm for computing slope and aspect from elevations. *Photogrammetric Engineering and Remote Sensing*, **35,** 247–248.

Shary, P. A., 1991, The second derivative topographic method. In *The Geometry of the Earth Surface Structures*, edited by I. N. Stepanov (Pushchino: Pushchino Research Centre Press), pp. 30–60 (in Russian).

Shary, P. A., 1995, Land surface in gravity points classification by complete system of curvatures. *Mathematical Geology*, **27,** 373–390.

Shary, P. A., Kuryakova, G. A., and Florinsky, I. V., 1991, On the international experience of topographic methods employment in landscape researches (the concise review). In *The Geometry of the Earth Surface Structures*, edited by I. N. Stepanov (Pushchino: Pushchino Research Centre Press), pp. 15–29 (in Russian).

Sobolevsky, P. K., 1932, The modern mining geometry. *Sotsialisticheskaya Reconstructsiya i Nauka*, **7,** 42–78 (in Russian).

Solovyev, V. V. (editor), 1977, *Map of Ring Morphostructures for the Territory of the USSR, scale 1:10000000* (Leningrad: Ministry of Geology of the USSR) (in Russian).

Speight, J. G., 1974, A parametric approach to landform regions. In *Progress in Geomorphology: Papers in Honour of D. L. Linton*, edited by E. H. Brown and R. S. Waters (London: Institute of British Geographers), pp. 213–230.

Stepanov, I. N. (editor), 1979, *Map of Quantitative and Qualitative Estimation of Salinization of Soils and Grounds (for the thickness of 1 metre) for Turkmenian Soviet Socialist Republic, scale 1:600000* (Moscow: The Central Board of Geodesy and Cartography of the Council of Ministers of the USSR) (in Russian).

Stepanov, I. N., 1986, *Forms in the World of Soils* (Moscow: Nauka) (in Russian).

Stepanov, I. N. (editor), 1989, *Map of Landsurface Systems and Soil Cover of the Part of the Middle Asia, scale 1:1500000* (Moscow: The Central Board of Geodesy and Cartography of the Council of Ministers of the USSR) (in Russian).

Suvorov, A. I. (editor), 1977a, *Faults and Horizontal Movements of Mountain Chain of the USSR* (Moscow: Nauka) (in Russian, with English contents).

Suvorov, A. I. (editor), 1977b, *Faults and Horizontal Movements of Platform Areas of the USSR* (Moscow: Nauka) (in Russian, with English contents).

Trifonov, V. G., Makarov, V. I., Safonov, Yu. G., and Florensky, P. V. (editors), 1983, *Space Information for Geology* (Moscow: Nauka) (in Russian, with English contents).

Troeh, F. R., 1964, Landform parameters correlated to soil drainage. *Soil Science Society of America Proceedings*, **28,** 808–812.

Yaroshenko, P. D., 1961, *Geobotany. The Main Conception and Methods* (Moscow: Soviet Academic Press) (in Russian).

Young, A., 1972, *Slopes* (Edinburgh: Oliver and Boyd).

Zevenbergen, L. W., and Thorne, C. R., 1987, Quantitative analysis of land surface topography. *Earth Surface Processes and Landforms*, **12,** 47–56.